Multiple Vortex Ring Model of the DFW Microburst

Thomas A. Schultz*
NASA Ames Research Center, Moffett Field, California

A multiple vortex ring model of the wind associated with a microburst is verified by matching model-generated wind to the wind encountered by American Airlines Flight 539 (AA539) in the 1985 Dallas-Fort Worth (DFW) microburst. The wind is modeled using time-invariant vortex ring filaments from potential flow theory. Each vortex ring filament is modified such that it is transformed into a viscous-core vortex ring. Parameters representing the size, position, and strength of the vortex rings are identified using a modified Newton-Raphson technique. The parameters identified from analysis of flight AA539's encounter with the DFW microburst indicate a large outer ring with a smaller inner ring near the center of the microburst. The outer ring has a diameter of 15,000 ft with a viscous core diameter of 4860 ft, and the inner ring has a diameter of 3200 ft with a viscous core diameter of 990 ft. The rms error between model-generated wind using two vortex rings and the wind encountered by flight AA539 at the DFW microburst is 10.4 ft/s.

Nomenclature

d = viscous core diameter
N = number of data points
R = vortex ring filament radius
v_x, v_y, v_z = wind velocity components
X, Y, Z = vortex ring position (runway coordinates)
x, y, z = position (runway coordinates)
Γ = vortex ring circulation strength
ζ = velocity damping factor
λ = stream-function parameter
ψ = stream function

Introduction

A MICROBURST is an intense downdraft which induces an outflow of strong wind near the ground.[1] This low-altitude windshear phenomenon continues to be a problem that must be investigated in the interest of aircraft safety.[2] Microburst wind encountered during landing or takeoff has been a contributing factor in several major commercial airline accidents. Current work addressing this problem includes microburst prediction and detection methods, and guidance and control strategies for flight through microbursts. For these efforts, it is essential to have a physically realistic mathematical model of the wind environment during a microburst.

Recently, there has been increased interest in the use of vortex rings to model the microburst. A vortex ring model for a microburst was first proposed from observations of the phenomenon.[3] It was suggested in Ref. 4 that vortex rings could be distributed in various ways to produce a flowfield that simulates a microburst. Studies which followed have made use of a single vortex ring.[5,6] The models of Refs. 5 and 6 were made to generate flowfields that resemble the flow patterns noted in the meteorological data of the Joint Airport Weather Study.[7] These wind data were collected using ground-fixed devices such as the Doppler radar and mesonet stations, which give large-scale information about the microburst. Neither of these studies includes airborne measurements from microburst windshear encounters, which provide additional information about wind fluctuations internal to microbursts.

Presented as Paper 88-0685 at the AIAA 26th Aerospace Sciences Meeting, Reno, NV, Jan. 11-14, 1988; received April 6, 1989; revision received Sept. 26, 1989.

*Aerospace Engineer. Member AIAA.

In August of 1985, two aircraft equipped with digital flight recorders penetrated a microburst that occurred at the Dallas-Fort Worth (DFW) airport. Digital flight recorder and air traffic control radar records were used to estimate the wind fluctuation along their flight paths.[8] The first aircraft, Delta Airlines Flight 191, penetrated the microburst during its landing approach and subsequently crashed. The following aircraft, American Airlines Flight 539, made a go-around and penetrated the same microburst during level flight at an altitude of about 2500 ft, and then proceeded to land safely.

Several models of the DFW microburst have been presented. The model of Ref. 9 uses an axisymmetric version of the Terminal Area Simulation System (TASS) to model the microburst. This numerical model considers the physics, dynamics, and time-dependent structure of the microburst and provides a means to explore the physical processes that create a microburst. The TASS model is initialized using Doppler radar measurements. The model presented in Ref. 10 is a simplified two-dimensional model of the DFW microburst, which was identified using wind estimates derived from flight recorder data. This model uses a combination of a source-sink pair, several vortex pairs, and a uniform horizontal bias to model the microburst flowfield.

The purpose of this study is to develop a simplified three-dimensional vortex ring model of an *isolated*[9] microburst. Using the AA539 wind data, a two-vortex-ring model is hypothesized in which the viscous core of each vortex ring is modeled by a continuous smooth function. A parameter identification (PID) technique is used to determine numerical values for the model parameters. The PID method utilizes the modified Newton-Raphson algorithm to identify model parameters that minimize the differences between the estimated wind of Ref. 8 and the modeled wind. This method was previously used to determine parameters in a vortex model of clear air turbulence.[11]

The hypothesized microburst model is presented, as well as a brief description of the estimation technique used to determine the model parameters. This is followed by a discussion of the results. It is shown that the multiple vortex ring model generates wind that closely approximates the wind observed at the DFW microburst.

Microburst Model

The hypothesized microburst model for this study consists of multiple vortex rings, each of which is modeled by a vortex ring filament that is derived from potential flow theory but

whose induced wind is modified by a velocity damping factor to account for the viscosity effects at the core of the vortex ring. Figure 1 shows a two-ring version of the multiple vortex ring model with viscous cores. The wind field for each vortex ring is given by the product of the wind induced by the ring filament and the velocity damping factor. The total wind field of the multiple vortex ring model is determined by summing the wind fields of the individual vortex rings. The development of the potential flow model and the damping factor for a single vortex ring are discussed below.

Potential Flow

The potential flow model for a single vortex ring in proximity to the ground is shown in Fig. 2. For each vortex ring filament above the ground plane, an image ring filament of the same size and strength is placed below the ground plane to make the ground plane a stream surface. Each vortex ring pair (primary and image) share a common central axis in the flowfield. Five parameters are required to fully describe the potential flow effects of each vortex ring pair. The first three parameters specify the position (X,Y,Z) of the center of the ring in the flowfield, and the other two specify the ring radius R and vortex circulation strength Γ. The x-y-z-coordinate system is referenced to the runway as shown in Fig. 2.

The wind induced by each vortex ring pair is computed by evaluating the derivatives of a combined vortex ring stream function ψ. The wind components induced at a point (x,y,z) by a vortex ring pair are given by

$$v_x = \left(\frac{x-X}{r^2}\right)\frac{\partial\psi}{\partial z} \tag{1a}$$

$$v_y = \left(\frac{y-Y}{r^2}\right)\frac{\partial\psi}{\partial z} \tag{1b}$$

$$v_z = \left(-\frac{1}{r}\right)\frac{\partial\psi}{\partial r} \tag{1c}$$

where r is the radial distance of the point from the central axis and is defined by

$$r = [(x-X)^2 + (y-Y)^2]^{1/2} \tag{2}$$

Fortunately, there exists a stream function representation for each vortex ring pair. The derivation of the vortex ring stream function is found in the classical test by Lamb.[12] The stream function contains an elliptic integral which can be approximated by an algebraic expression as pointed out in Ref. 6. The stream function for the vortex-ring pair using the algebraic approximation is given by

$$\psi \approx \sigma\left[\frac{(a_1+a_2)\lambda_a^2}{1+3(1-\lambda_a^2)^{1/2}} - \frac{(s_1+s_2)\lambda_s^2}{1+3(1-\lambda_s^2)^{1/2}}\right] \tag{3}$$

where

$$a_1 = [(z-Z)^2 + (r-R)^2]^{1/2} \tag{4a}$$

$$a_2 = [(z-Z)^2 + (r+R)^2]^{1/2} \tag{4b}$$

$$s_1 = [(z+Z)^2 + (r-R)^2]^{1/2} \tag{5a}$$

$$s_2 = [(z+Z)^2 + (r+R)^2]^{1/2} \tag{5b}$$

$$\lambda_a = (a_2-a_1)/(a_2+a_1) \tag{6a}$$

$$\lambda_s = (s_2-s_1)/(s_2+s_1) \tag{6b}$$

$$\sigma = 1.576\Gamma/\pi \tag{7}$$

The variables a_1 and a_2 represent the closest and farthest distance, respectively, from the point of interest (x,y,z) to the primary vortex ring filament. These distances lie in the plane that contains the point of interest and the central axis. Similarly, the variables s_1 and s_2 represent the closest and farthest distances, respectively, to the corresponding image ring. The terms λ_a and λ_s are scaling terms used in the algebraic evaluation of the elliptic integral.[12]

At the point (x,y,z) in the flowfield, the algebraic expression for the induced wind as a function of the vortex ring position (X,Y,Z), the filament radius R, and the circulation strength Γ can be obtained by substituting the required partial derivatives of the stream function $(\partial\psi/\partial z, \partial\psi/\partial r)$ into Eq. (1). The algebraic expressions for the stream function derivatives are given in the Appendix. The expressions for the wind components in Eq. (1) are valid everywhere except at the vortex ring filament and at the vortex ring's central axis. In either of these two regions, the numerical evaluation of the wind components [Eq. (1)] would result in a singularity (i.e., division by 0). Thus, the singularities of Eq. (1) will be removed by using different equations in the singular regions of Eq. (1).

Figure 3 illustrates the singularity in Eq. (1) at the filament, for the case where an aircraft passes through the vortex ring filament. The lower part of Fig. 3 shows the vertical wind encountered along the flight path; notice that the wind component approaches infinity near the filament. To remove the singularity at the filament, the magnitude of the wind at the

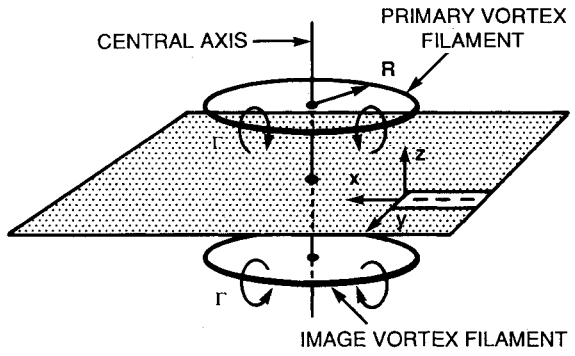

Fig. 2 Potential flow parameters of a primary-image ring pair.

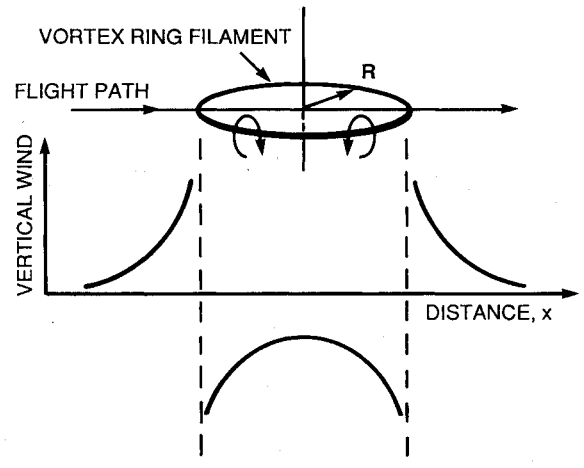

Fig. 3 Potential flow model singularity is demonstrated by the wind induced along a trajectory through a vortex filament.

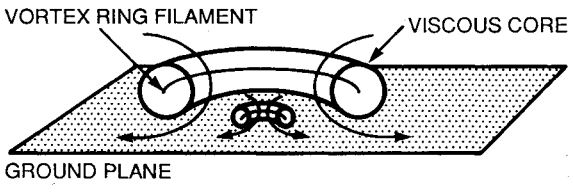

Fig. 1 Multiple vortex ring model using two rings with viscous cores.

filament is set to zero. The viscous core modification discussed in the next section will insure a continuous induced wind function with zero magnitude at the location of the vortex ring filament.

The singularity at the central axis is removed by setting the wind induced at the central axis equal to the limit solution. Equation (8) gives the limit solution for the wind at the central axis (Fig. 2) of the vortex ring pair.[13]

$$v_x = 0 \tag{8a}$$

$$v_y = 0 \tag{8b}$$

$$v_z = \frac{\Gamma R^2}{2}\{[R^2 + (Z+z)^2]^{-3/2} - [R^2 + (Z-z)^2]^{-3/2}\} \tag{8c}$$

Viscous Core Modification

Because of the viscous nature of air, potential flow theory alone cannot adequately model the microburst wind environment. It is the viscosity that creates the measurable cores of the microburst's vortex rings and keeps the actual flowfield from becoming singular. The viscosity effects are included by modifying the potential flow model with a velocity damping factor.

By modifying the potential flow-induced wind near the vortex filament with a velocity damping factor, the vortex filament is replaced with a core of finite dimensions. This core is labeled the "viscous core" because the core's radial velocity distribution resembles the distribution of a spreading line vortex in a viscous medium.[14] This viscous core modification to potential flow theory creates a model that provides a good match between observed and modeled wind.

From a fluid dynamic point of view, the viscous core of a vortex ring is modeled by distributing the vorticity away from its concentration at the vortex filament. Distributing the vorticity over a small distance (relative to the ring radius R) radially from each filament does not reduce the net circulation of the ring system, nor does it affect the wind induced at distances far away from the filaments. This is because the distribution of vorticity is confined to the vicinity of the vortex filament.

Figure 4 illustrates the vertical wind inside the viscous core, for the case where the aircraft penetrates the center of the core. The vertical winds encountered while flying through the viscous core (solid line in Fig. 4) are superimposed on the unmodified potential flow winds (broken line in Fig. 4) reproduced from Fig. 3. The velocity damping factor ζ is empirically derived so that when it multiplies the potential-flow-derived wind field [Eq. (1)], a viscous core vortex ring is obtained. After the modification, the wind velocity becomes continuous everywhere in the flowfield.

Because the velocity damping factor alters the potential flow wind distribution to resemble the velocity distribution of a spreading line vortex, the damping factor has the same mathematical form as a factor in the solution for a spreading line vortex.[14] The expression for the damping factor is given by

$$\zeta = 1 - \exp\left\{ - \frac{\left(\frac{a_1}{R}\right)^2}{\left[0.4215\frac{d}{R} + 0.0822\left(\frac{d}{R}\right)^2 - 0.0969\left(\frac{d}{R}\right)^3\right]^2} \right\} \tag{9}$$

Note that the damping factor equation is a smooth function of three parameters: the core diameter d, the ring radius of the filament R, and the closest distance from point (x,y,z) to the filament a_1. The denominator of the exponent's argument in Eq. (9) was developed empirically to allow the core diameter d to directly govern the size and shape of the viscous core. The three-dimensional nature of the model is also taken into account in the damping factor expression [Eq. (9)] via the vortex ring filament radius R. Notice how the damping factor's dependence on the vortex ring radius R diminishes as the vortex ring becomes large relative to the core diameter.

The damping factor ζ ranges between 1 and 0. When the point of interest is far away from the primary vortex ring's viscous core, the viscous core has no effect on the induced wind at that point in the flowfield, and $\zeta = 1$. In this case, the potential flow theory and the modified potential flow theory produce the same results. When the point of interest is at the center of a primary ring's viscous core, the induced wind is zero, and $\zeta = 0$. Zero induced wind at the core's center is consistent with the assumption that the model is time invariant.

Use of the modified potential flow-induced wind adds one additional parameter for each vortex ring pair. The viscous core diameter d is the sixth parameter required to model a vortex ring pair. The parameter vector for a vortex pair is $(X,Y,Z,R,d,\Gamma)^T$.

Estimation Technique

When trying to match the multiple vortex ring model to a microburst wind field, the analyst is free to choose the number of rings to be used in the model after inspection of the microburst wind data. The number of parameters required to specify the multiple vortex ring model increases by six for each vortex ring pair in the flowfield. From visual inspection of the microburst wind data, the analyst can obtain initial estimates of the parameters. A parameter-estimation algorithm will then determine the numerical values of the model parameters, which minimizes the differences between modeled wind and observed or estimated wind.

The unknown model parameters are determined by minimizing the squared-error cost function J as follows:

$$J = \frac{1}{N}\sum_{j=1}^{N} \boldsymbol{e}_j^T(\boldsymbol{p})\boldsymbol{B}\boldsymbol{e}_j(\boldsymbol{p}) \tag{10}$$

where N is the number of data points, $\boldsymbol{B}$ is the weighting matrix, $\boldsymbol{e}_j(\boldsymbol{p})$ is the error between the actual and the modeled wind at the time point j, and $\boldsymbol{p}$ is the parameter vector. The error vector is

$$\mathbf{e}(\boldsymbol{p}) = \boldsymbol{V}_a - \boldsymbol{V}_m \tag{11}$$

where $\boldsymbol{V}_a$ is the actual wind observed along the flight path and $\boldsymbol{V}_m$ is the modeled wind, and

$$\boldsymbol{V}_a = [v_x v_y v_z]_a^T, \qquad \boldsymbol{V}_m = [v_x v_y v_z]_m^T \tag{12}$$

The parameter vector $\boldsymbol{p}$ is defined as

$$\boldsymbol{p} \equiv [X\,|\,Y\,|\,Z\,|\,R\,|\,d\,|\,\Gamma]^T \tag{13}$$

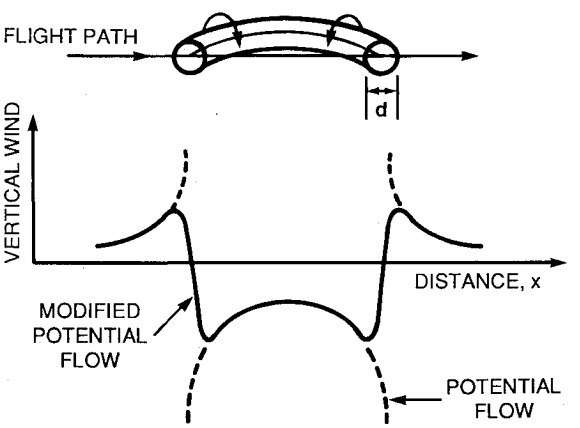

Fig. 4 Viscous core modification of a vortex ring.

with

$$X \equiv [X_1,\ldots, X_i, \ldots, X_N], \quad Y \equiv [Y_1,\ldots, Y_i,\ldots, Y_N] \quad (14a)$$

$$Z \equiv [Z_1,\ldots, Z_i,\ldots, Z_N], \quad R \equiv [R_1,\ldots, R_i,\ldots, R_N] \quad (14b)$$

$$d \equiv [d_1,\ldots, d_i,\ldots, d_N], \quad \Gamma \equiv [\Gamma_1,\ldots, \Gamma_i,\ldots, \Gamma_N] \quad (14c)$$

where i refers to the ith vortex ring pair.

The Newton-Raphson algorithm, which is given in Ref. 11, is used to minimize J in Eq. (10). The algorithm requires calculation of error sensitivities to find improved parameter estimates. Previous modeling efforts with vortex arrays[11] which use solid-body cores result in discontinuities at the ring boundaries, further complicating the identification of core diameters. The multiple vortex ring model consisting of Eqs. (1), (8), and (9) is a smooth, continuous function and well suited for use with the PID technique.

Application to DFW Microburst Data

During the DFW microburst, AA539 made a go-around 110 s after the Delta 191 accident and penetrated the microburst flying level at an altitude of 2500 ft above the ground. Estimates of the wind and position-time histories (x,y,z) of both aircraft can be found in Ref. 8. In this study, it was of interest to model the DFW microburst at the time when it was penetrated by AA539, so only the AA539 data was used for this model. As AA539 traversed the microburst, the horizontal y component of the wind showed a linear change. This effect could have been caused by a cyclonic rotation of the microburst. A plot of the y component of the wind is presented in Ref. 8. For the present analysis, however, the cyclonic rotation was not modeled, and therefore the y component of the wind was not used in the analysis.

The PID technique described in the previous section requires as input the number of vortex ring pairs in the model, and initial estimates of the model parameters $(X,Y,Z,R,d,\Gamma)^T$ for each vortex ring pair; these are obtained by visual inspection of the vertical wind estimates shown in Fig. 5. The shape of the modified potential-flow velocity profile shown in Fig. 4 is key to visually selecting the number of vortex ring pairs needed to match observed data in the microburst flowfield. Comparison of the velocity profile in Fig. 4 (solid line) with the vertical wind in Fig. 5 suggests that the wind in Fig. 5 may be approximated by superposition of two vortex rings, the smaller of the two rings being near the axis of symmetry (central axis) of the larger one.

Initial estimates of the microburst size and circulation strength parameters (R,d,Γ) for each vortex ring pair were obtained by visual inspection. The small ring was estimated to have a viscous core diameter of 900 ft and a ring diameter of 2500 ft; the large ring was estimated to have a viscous core diameter of 3000 ft and a ring diameter of 15,000 ft. An initial estimate for each ring's circulation is made by multiplying the ring diameter by an estimate of the vertical wind induced at the central axis of the ring. This relationship can be verified by solving the Γ using the second term in Eq. (8). The induced vertical wind along the central axis for both of the rings is about -15 ft/s. Using the above vortex ring diameter estimates results in initial circulation estimates of 225,000 ft^2/s for the large ring and 37,500 ft^2/s for the small ring.

An initial estimate for the (X,Y,Z) position of each vortex ring is obtained by assuming that the aircraft flew directly through the center of the microburst. The X component of the vortex rings is selected visually from Fig. 5. The vertical wind in Fig. 5 shows a rough symmetry of about 10,380 ft; therefore, 10,380 ft was chosen as the X position for both vortex rings. The Y and Z components corresponding to $X = 10{,}380$ ft are obtained from the estimated position-time history and are -300 ft and 2500 ft, respectively. Because the y component of the estimated wind was not used in this analysis, for reasons mentioned earlier, there is not enough information to identify the Y position component of both vortex rings; so the Y component of both rings is fixed at the initial estimate of -300 ft throughout the analysis.

From the initial parameters summarized in Table 1, the PID technique was used to determine the final set of parameter estimates shown in Table 2. The cost-function [Eq. (10)] minimization was done using equal weights on the x and z components of the wind, and no weight on the y component. The initial rms error between the measured wind (or the estimated wind, in Ref. 8) and the modeled wind was 20 ft/s, and after the minimization process the rms error was 10.4 ft/s. The microburst wind generated from the model using the improved parameters is plotted in Fig. 6 along with the x and z measured components of the wind. The identification procedure incorporating the multiple vortex ring model proved to be robust (i.e., the final parameter values identified were not very sensitive to the choice of initial estimates). This robustness is primarily the result of two things: 1) the microburst model has the property of being a smooth function, and 2) the vertical wind data have variations that resemble the wind profile of the superposition of the vertical wind profiles from two vortex rings.

Discussion

The previous analysis strongly suggests that AA539 flew through the viscous core of both rings, slightly below the larger

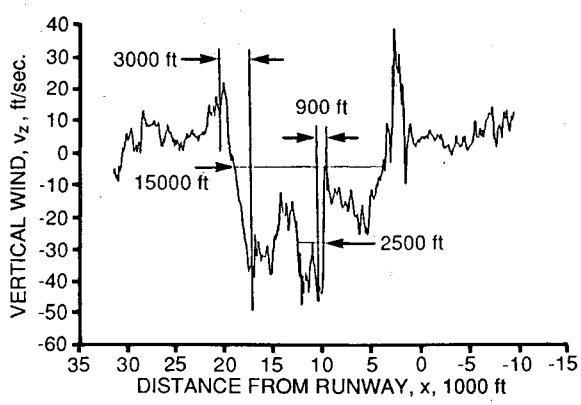

Fig. 5 Vertical wind encountered by AA539 flying through a microburst at 2500 ft in level flight.

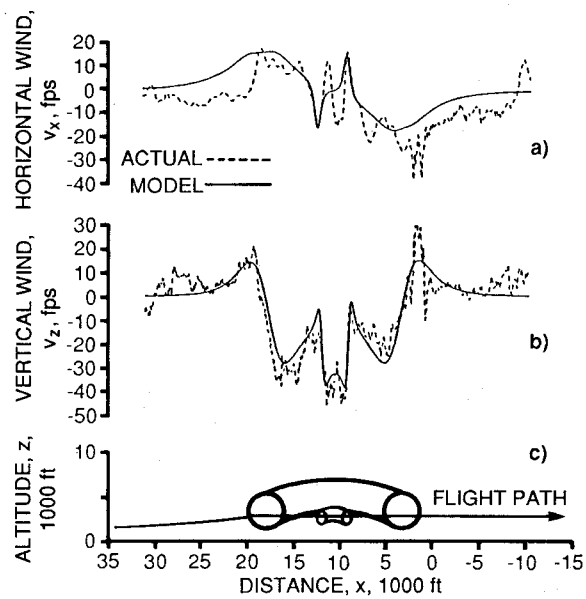

Fig. 6 Winds calculated from the multiple vortex ring model along with the winds encountered by AA539.

Table 1 Initial estimates of microburst model parameters

Parameter	Large ring	Small ring
Ring radius, ft	7,500.0	1,250.0
Core diameter, ft	3,000.0	900.0
Ring circulation, ft^2/s	225,000.0	37,500.0
X position, ft	10,380.0	10,380.0
Y position, ft	−300.0	−300.0
Z position, ft	2,500.0	2,500.0

Table 2 Final estimates of microburst model parameters

Parameter	Large ring	Small ring
Ring radius, ft	7,574.0	1,594.3
Core diameter, ft	4,856.8	985.0
Ring circulation, ft^2/s	434,360.3	63,670.1
X position, ft	10,711.7	10,649.9
Y position, ft	−300.0	−300.0
Z position, ft	3,394.7	2,305.6

ring's center and slightly above the smaller ring's center (see Fig. 6c).

The longitudinal v_x and vertical v_z wind components in Fig. 6 show that the aircraft experienced an increasing head wind and an updraft as it approached the microburst's large ring. Once inside the large ring's core, the aircraft experienced an increase in downdraft as it flew to the other side of the core, while the head wind remained constant. After leaving the viscous core of the large ring, the aircraft experienced a decrease in the downdraft magnitude and the head wind changed into a tail wind until the aircraft entered the viscous core of the small ring. As the aircraft flew through the small ring, it experienced first an increase and then a decrease in downdraft, which was matched by the model. However, the head wind modeled inside the small ring does not fit the data, whereas the modeled wind for the rest of the encounter shows excellent agreement. After the airplane left the small ring, it again experienced an increase in downdraft, and an increase in tail wind, until it reached the viscous core on the other side of the large ring. Inside the large ring's core, the tail wind remained constant and the downdraft turned to an updraft. Finally, the aircraft left the viscous core, the updraft died out, and the tail wind diminished.

The multiple vortex ring model is designed to model the average large-scale wind velocity fluctuations in a microburst. The aim of this vortex model is to capture the main characteristics of a microburst so that the effects on aircraft performance and control strategies can be better understood. From examination of the AA539 data, the two-vortex ring model provides a good representation of the downdraft, the strong shift from head wind to tail wind, and the vertical wind fluctuations observed internal to the microburst during the flight of AA539.

An extension of the model would allow the rings to be tilted or moved relative to one another. Vortex rings induce their own translational motion and are influenced by the lift-cycle dynamics of the microburst which were described in Ref. 15 and dynamically modeled in Ref. 16. This model and estimation technique might be applied to other types of wind measurements (e.g., those from ground-based Doppler radar). However, these other measurements may not be precise enough to provide information about the smaller embedded rings, such as was available from digital flight records from the DFW encounter.

Concluding Remarks

A multiple vortex ring model was developed from the application of a vortex ring stream function. The wind induced by each vortex ring is calculated by evaluating an algebraic expression representing the derivatives of its stream function. This wind is then multiplied by the velocity damping factor used to model the viscous core of the rings. The wind at any position in the flowfield is the sum of the winds induced at that position by each ring present, including the image rings.

This multiple vortex ring model was verified by matching model-generated wind to the actual wind estimated from an aircraft penetrating a microburst. A Newton-Raphson scheme was used to determine the model parameters to represent the DFW microburst, which was measured by AA539. The results show a large ring with a smaller inner ring embedded in the downflow. The multiple vortex ring model provides a realistic representation of the microburst wind field and can be used in simulation and control system studies.

Appendix: Stream Function Derivatives

Differentiating Eq. (3) with respect to r and z yields the following expressions for $\partial\psi/\partial z$ and $\partial\psi/\partial r$:

$$\frac{\partial\psi}{\partial z} = -2\sigma\left(\frac{z+Z}{s_2} - \frac{z+Z}{s_1}\right)\eta_s + \sigma\left(\frac{3(z+Z)s_2^{1/2}}{s_1^{3/2}} + \frac{z+Z}{s_2} + \frac{3(z+Z)s_1^{1/2}}{s_2^{3/2}} + \frac{z+Z}{s_1}\right)\eta_s^2 - \sigma\left(\frac{3(z-Z)a_2^{1/2}}{a_1^{3/2}} + \frac{z-Z}{a_2} + \frac{3(z-Z)a_1^{1/2}}{a_2^{3/2}} + \frac{z-Z}{a_1}\right)\eta_a^2 + 2\sigma\left(\frac{z-Z}{a_2} - \frac{z-Z}{a_1}\right)\eta_a \tag{A1}$$

$$\frac{\partial\psi}{\partial r} = -2\sigma\left(\frac{r+R}{s_2} - \frac{r-R}{s_1}\right)\eta_s + \sigma\left(\frac{3(r-R)s_2^{1/2}}{s_1^{3/2}} + \frac{r+R}{s_2} + \frac{3(r+R)s_1^{1/2}}{s_2^{3/2}} + \frac{r-R}{s_1}\right)\eta_s^2 - \sigma\left(\frac{3(r-R)a_2^{1/2}}{a_1^{3/2}} + \frac{r+R}{a_2} + \frac{3(r+R)a_1^{1/2}}{a_2^{3/2}} + \frac{r-R}{a_1}\right)\eta_a^2 + 2\sigma\left(\frac{r+R}{a_2} - \frac{r-R}{a_1}\right)\eta_a \tag{A2}$$

where

$$\eta_a = \frac{(a_2-a_1)}{(a_2+6\sqrt{a_2a_1}+a_1)}, \qquad \eta_s = \frac{(s_2-s_1)}{(s_2+6\sqrt{s_2s_1}+s_1)} \tag{A3}$$

The terms a_1, a_2, s_1, and s_2 are defined in Eqs. (4) and (5), and σ is defined in Eq. (7).

Acknowledgments

The author thanks Rajiv Mehta for his guidance in adapting the parameter-estimation technique that he developed for modeling clear-air turbulence. The author also thanks E. K. Parks for suggestions about modeling the DFW microburst with vortex rings.

References

[1]Fujita, T. T., "The Downburst," SMRP Research Paper 210, Univ. of Chicago, Chicago, IL, 1985.

[2]*Low-Altitude Wind Shear and Its Hazard to Aviation*, National Academy of Sciences, National Academy Press, Washington, D.C., 1983.

[3]Caracena, F., "Is the Microburst a Large Vortex Ring Imbedded in a Thunderstorm Downdraft?" Transactions of the American Geophysics Union, Vol. 63, No. 45, 1982, p. 89.

[4]Etkin, B., "A Model of a Downburst; A Wind-Tunnel Program on Planetary Boundary Layer; and Airship in Turbulence." NASA CP-2312, April 1984.

[5]Woodfield, A., "Real-time Simulation of Thunderstorm Windshear, Turbulence, and Steady Wind," Royal Aircraft Establishment, Bedford, England, May 1984.

[6]Ivan, M., "A Ring-Vortex Downburst Model for Flight Simulations," *Journal of Aircraft*, Vol. 23, March 1986, pp. 232–236.
[7]"The JAWS Project Preliminary Data Description," National Center for Atmospheric Research, Boulder, CO, Sept. 1983.
[8]Wingrove, R. C. and Bach, R. E., "Severe Winds in the DFW Microburst Measured from Two Aircraft," AIAA Paper 87-2340-CP, Aug. 1987.
[9]Proctor, F. H., "Numerical Simulations of an Isolated Microburst. Pt. I: Dynamics and Structure," *Journal of Atmospheric Sciences*, Vol. 45, No. 21, Nov. 1988, pp. 3137–3160.
[10]Grantham, W. J., "The DFW Microburst: A Two-Dimensional Multiple Vortex Model," AIAA 26th Aerospace Sciences Meeting, AIAA, Washington, DC, Jan. 11–14, 1988.
[11]Mehta, R. S., "Modeling Clear-Air Turbulence with Vortices Using Parameter-Identification Techniques," AIAA Paper 84-2083, Aug. 1984.
[12]Lamb, H., *Hydrodynamics*, Dover, New York, 1932, pp. 236–243.
[13]Duncan, W. J., Thom, A. S., and Young, A. D., *Mechanics of Fluid*, American Elsevier, New York, 1960, p. 93.
[14]Batchelor, G. K., *An Introduction to Fluid Dynamics*, Cambridge University Press, Cambridge, England, UK, 1967, p. 204.
[15]McCarthy, J., "Microburst Wind Shear: An Aviation Hazard," *Proceedings of 36th International Air Safety Seminar*, Nov. 1983.
[16]Proctor, F. H., "The Terminal Area Simulation System," *Verification Cases*, Vol. II, NASA CR-4047, 1987.